Simulation study of furnace temperature field reconstruction based on acoustic tomography

Simulation study of temperature field reconstruction based on acoustic tomography

Yong Bao, Jiabin Jia, Nick Polydorides

School of Engineering, University of Edinburgh, Edinburgh, EH9 3JL, UK
{y.bao Jiabin.Jia N.Polydorides}@ed.ac.uk

ABSTRACT

To improve the understanding of the combustion process and evaluating the combustion efficiency, temperature of flame is monitored. The conventional temperature measurements methods, like thermocouple and thermometer, can only provide pointwise estimation from their invasive measurement. Vision-based monitoring techniques heavily rely on the optical access into the process, and it is only suitable for some specific applications which allow opening observation window at the boundary. A study in this paper aims to reconstruct the 2D temperature field in the furnace using acoustic tomography. Compared with other methods, acoustic tomography gives the global estimation of the temperature field with a good accuracy. In this tomographic modality, acoustic transducer and receivers are placed around the temperature field to estimate sound speed within the flame region using time-of-flight (TOF) method, from which the temperature field can be derived. In this paper, the entire process of obtaining temperature filed is introduced. A simulation study is given by coupling two physical fields, temperature and acoustic pressure fields based on COMSOL Multiphysics. As the reconstruction quality suffers from the lack of measurements, and the inverse problem is always ill-posed, the temperature field is modelled by a sum of radial basis functions (RBF) and then a TSVD method is used to solve the inverse problem. The possible error sources are analysed. Three test scenarios demonstrated acoustic tomography is able to reconstruct temperature field with reasonable accuracy.

Keywords Acoustic sound speed tomography, parametric temperature field, reconstruction methods, TOF detection.

1 INTRODUCTION OF ACOUSTIC TOMOGRAPHY

Acoustic Tomography (AT) was firstly used to monitor ocean structure (Munk 1982) and then applied in temperature field reconstruction by Spiesbergerin (1990) and Wilson (1994). According to the strong dependence of sound propagation on the temperature and velocity of the medium, AT is also used to reconstruct temperature and velocity distribution in the measurement region (Barth 2013 and Yan 2013).

A typical AT system setup is illustrated in Figure 1. The field of interest is surrounded by 16 acoustic transducers. The 120 straight acoustic rays travel between different pairs of transducers and their Time-Of-Flight (TOF) measurements enable an accurate estimation for the sound speed within the sensing area. Eventually temperature field distribution is derived from these sound speed measurement. Many researches showed that AT could achieve good results for temperature field reconstruction (Jovanovic 2006 and Rogers 2012). However these high quality reconstructions are based on a temperature field in atmosphere where the variation of temperature is small. Applying AT to monitoring the furnace brings more challenging. First, in most AT system, temperature field does not have large fluctuation, which is a key factor to ensure a good reconstruction quality, however in the furnace, there is always sharp peak in the temperature field. In addition, there is a hard boundary around the sensing area, which will cause multiple reflections during acoustic wave propagation and distortion in the received signal.

The temperature estimation is known to be a scalar tomography problem in the sense that it recovers a scalar function from its line integrals. This integral can be computed from the time taken by a sound wave to propagate from a transmitter to a receiver, namely TOF t, defined in (1).

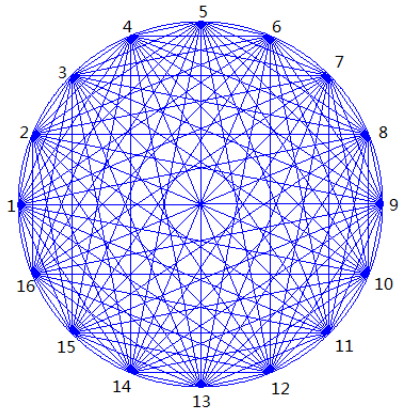

Figure 1. Simulation setup with 16 acoustic transducers

$$t = \int_l \frac{dl}{c} \tag{1}$$

where c represents the sound speed, l is the ray path of acoustic propagation. Equation (1) is always linearized before reconstruction, since it can be approximated as the first order expansion of the function (Jovanovic 2006):

$$t = \int_l \frac{dl}{c_0 + \Delta c} \approx \frac{L}{c_0} - \frac{1}{{c_0}^2} \int_l \Delta c \, dl \tag{2}$$

This approximation is feasible only when the fluctuation of sound speed is small with compared to its mean value, i.e. $\Delta c \ll c_0$. However, this may not be valid when temperature field change is relatively large (Liu 2015). Instead of using the sound speed, the slowness of sound propagation is used, which equals to the reciprocal of the sound speed (c=1/s). The TOF t is the line integral of the slowness of sound propagation as shown in (3), then temperature field is estimated from the slowness field.

$$t = \int_l s \, dl \tag{3}$$

For homogenous ideal gas properties of air, the relation between sound speed c and temperature T is defined in (4).

$$c = \frac{1}{s} = \sqrt{R\gamma T} \tag{4}$$

where R is the gas constant and specific heat ratio $\gamma = 1.4$. In order to use algebraic-based algorithms for reconstruction, temperature is firstly discretized into small grids, and temperature and sound speed are assumed constant within each pixel. Then a discrete equation for TOF is expressed as

$$t_m = \sum l_{mn} \, s_n \tag{5}$$

where t_m is the TOF for m-th ray path, l_{mn} is the segment length for m-th ray path in n-th pixel, c_n is the corresponding sound speed. TOF and slowness between all the transmitters and receivers are written in the form of array $g = [t_1, t_2, t_3, t_4, \dots, t_M]$ and $s = [s_1, s_2, s_3, \dots, s_N,]$ respectively. The relation of g and s is defined in (6).

$$g = As \tag{6}$$

The element of mapping matrix A is $A_{mn} = l_{mn}$ and M and N are the number of ray path and pixel grids respectively. The equation (6) leads to a linear inverse problem to reconstruct the slowness of sound speed s for the further estimation of temperature, given that TOF measurements g and system matrix A are determined by the experiment setup.

2 SIMULATION

This section focuses on solving forward problem of AT in FEM simulation environment COMSOL Multiphysics, including the temperature field simulation and pressure acoustic study. Firstly the time-dependent heat transfer module is built to provide more realistic temperature field phantom of furnace in different situations, then pressure acoustic module is coupled to simulate the acoustic sensors and the received signals. The computed TOFs are used for reconstructing temperature field.

2.1 Theory Background

In this simulation, the acoustic wave propagation is studied in an ideal isentropic process, where all the thermodynamic process are assumed reversible and adiabatic. Besides the acoustic signal is regarded as a longitudinal wave, a flow of energy with rapid change above a static value, which is the atmosphere pressure. The governing equation below is based on the conservation of mass and momentum (Rjenstra 2003):

$$\frac{1}{\rho_0 c_s^2}\frac{\partial^2 P'}{\partial t^2} + \nabla \cdot \left(-\frac{1}{\rho_0}\nabla p'\right) = 0 \tag{7}$$

where ρ the total density, p is the total pressure, and u is the velocity field. The small parameter expansion P' is performed at pressure p_0 (SI unit: Pa), c_s is the sound speed of acoustic signals.

2.2 Simulation Setup

The material of sensors is set as Lead Zirconate Titanate (PZT-5H) and the region of interest is filled with dry air. The diameter of sensing area is 1m, and sensors size is 0.01m*0.005m. A Gaussian pulse is selected to be the source signal, with bandwidth of 1 kHz and duration of 1ms. During the simulation, the sensors take turns to transmit acoustic waves into the air, then signals on all other sensors are recorded. It takes about 5ms to complete acoustic signal transmitting and receiving among all the transducers, therefore, temperature field is assumed to be constant during this period of time.

The heat transfer module uses a 1000W line heat source and all the boundary are set to be ideal thermal isolation. The model is simulated for 1000s in COMSOL and temperature field is obtained at the end of 1000s. Coupled with the heat transfer module, pressure acoustic module simulates the acoustic pressure field. A linear elastic model is selected for modelling the ideal gas. The boundary of the sensing area is set to be a hard wall for acoustic pressure field, so that acoustic wave reflection with a phase shift occurs in this model.

For the transmitter and source signal, the piezoe-acoustic transducer is initially tested in the simulation, which transforms an electric current to an acoustic pressure field, or vice versa. However, it is very difficult to generate the desired waveform of transmitted signal using the piezoe-acoustic transducer, because the output signal is determined not only by the input current but also the size and the material of transducer. Without careful design, the transmitter will generate a distorted waveform. Later, a time-dependent pressure boundary is adopted to give the Gaussian pulse signal on the sensor surface of acoustic transmitter.

2.3 Mesh

The solution to acoustic problems is wavelike and it can be resolved by predefined mesh. The size of mesh is determined by the wavelength. The wave is characterized by a wavelength λ in space, whose value depends on the frequency f and speed of sound c in the medium according to $\lambda = c/f$. This wavelength has to be resolved by the mesh. Due to Nyquist's law we need at least 2 degrees of freedom per wavelength, but in order to get a high-quality simulation, 5 to 10 degree-of-freedom per wavelength is used here. As the propagation direction is unknown beforehand, an isotropic mesh is needed. Here we choose Free Tetrahedral mesh, and set maximum element size to be $c/(10 * f)$.

3 TIME-OF-FLIGHT (TOF) PICKER

The accuracy of TOF measurements greatly influences the quality of reconstruction image. Many TOF pickers have been invented in the past decades, and these techniques fall into two categories. The first one is based on first arrival detection. It measures the significant change in the received signal and regards the changing points as the arrival time of the acoustic signal. Common way to implement this is to apply a threshold detection at the receiver, but this method suffers from the noise and requires a strong prior knowledge to determine the threshold value. Other first arrival detection methods apply a running window to cover one signal segment, then calculate the value of a predefined function to characterize signal within the window. The change of the function value instead of signal amplitude is used to estimate the right TOF points (Li 2009).

However all these methods are based on an assumption that the changing point correctly indicates the arrival time of acoustic signal, but actually this is not always true, because the acoustic signal is longitudinal wave, and at the receiver side acoustic pressure starts to change before the wave front arrives. First arrival detection always incurs an error in estimating the true TOF, and this issue cannot be ignored.

Another method mainly uses coherence characteristic between the source signal and the received signal, assuming that the received signal has the similar waveform of source signal without much distortion. The cross-correlation function is defined as

$$R(\tau) = lim_{T\to\infty} \frac{1}{T} \int_0^T f_s(t)\, f_r(t+\tau) \tag{8}$$

where $f_s(t)$ is the transmitted acoustic signal and $f_r(t)$ is the received signal. Normally, the largest cross-correlation $R(\tau)$ is picked from the series, and the corresponding τ is the TOF point. However, this may fail to give the right results as there may be multiple reflection waves within the received signal. As demonstrated in Figure 3(a) below, in some situation the reflected waves give the largest cross-correlation value.

Instead of finding the global maximum point, we try to find all the peaks of correlation graph, which are the local maximum with $\mathrm{dR}/\mathrm{d}\tau = 0$. This criteria by searching local maximum is sensitive to noise so that a median filter is necessary to remove outliers. Besides, the TOF should always be positive, all the peaks for negative τ should be ignored, and finally choose the first peak corresponding to directly propagated signal.

To validate the performance, the algorithm is tested under a room temperature field, where temperature is 293.15 K and corresponding sound speed is 343m/s. with a known distance between the transducer No. 1 and the receiver No. 7 in simulation setup Figure 1, the true TOF can be calculated. The received signal on the receiver No. 7 is displayed in Figure 3(b). The green vertical line represents the true TOF point, and the red one is the TOF picker result from the cross-correlation algorithm. In Figure 3(a) there are two major peaks of the cross-correlation values, which are associated with the direct wave and reflection respectively. The first peak is selected to calculate the TOF point and the analytical result and the calculation result have a good agreement.

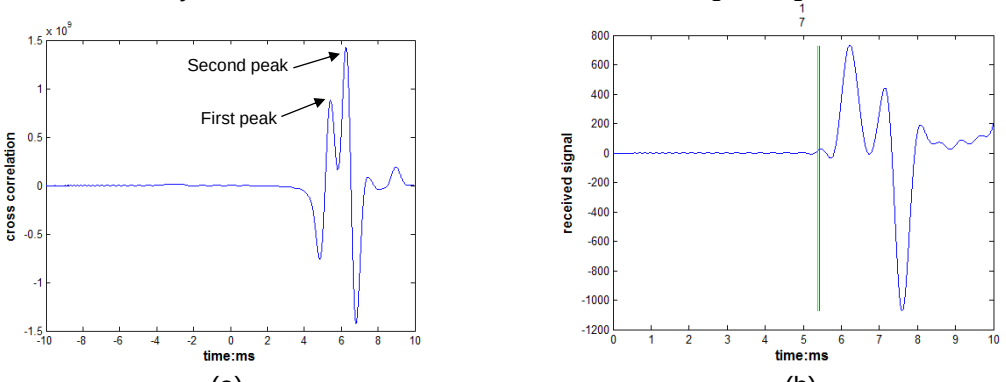

(a) (b)

Figure 3. Cross-correlation coefficients (a) and TOF picker results (b) between transmitter No.1 and receiver No.7

The TOF measurement error for all transmitter and receiver pairs are listed in Table 1. From this table we can find when large TOF measurement errors mainly occur when the direct and reflection wave are close to each other, the cross-correlation method cannot distinguish them very well. The worst case is marked in red shadow. In fact, all of them are from transducer-receiver pairs whose angle is about 112.5°.

The cross-correlation series of the transmitter No.1 and the receiver No. 6 is shown in Figure 4(a). The received signal on the receiver No. 6 is displayed in Figure 4(b). Compared with Figure 3, the overlap of the direct wave and reflection wave causes larger estimation error of TOF point.

Table 1. TOF measurement error between different transmitter and receiver pairs

	R1	R2	R3	R4	R5	R6	R7	R8	R9	R10	R11	R12	R13	R14	R15	R16
T1	0	0.038	0.004	0.007	0.024	0.061	0.01	0.011	0.011	0.01	0.01	0.061	0.024	0.007	0.004	0.038
T2	0.038	0	0.038	0.004	0.007	0.024	0.063	0.01	0.01	0.011	0.01	0.01	0.061	0.024	0.007	0.004
T3	0.004	0.038	0	0.038	0.004	0.007	0.024	0.061	0.01	0.011	0.011	0.011	0.01	0.061	0.024	0.007
T4	0.007	0.004	0.038	0	0.038	0.004	0.007	0.024	0.061	0.01	0.01	0.011	0.011	0.01	0.063	0.024
T5	0.024	0.007	0.004	0.038	0	0.038	0.004	0.007	0.024	0.063	0.01	0.01	0.011	0.01	0.01	0.061
T6	0.061	0.024	0.007	0.004	0.038	0	0.038	0.004	0.007	0.024	0.061	0.01	0.01	0.011	0.01	0.01
T7	0.01	0.063	0.024	0.007	0.004	0.038	0	0.038	0.004	0.007	0.024	0.063	0.01	0.01	0.011	0.01
T8	0.01	0.01	0.063	0.024	0.007	0.004	0.038	0	0.038	0.004	0.007	0.024	0.063	0.01	0.01	0.011
T9	0.011	0.01	0.01	0.061	0.024	0.007	0.004	0.038	0	0.038	0.004	0.007	0.024	0.063	0.009	0.01
T10	0.01	0.011	0.01	0.01	0.063	0.024	0.007	0.004	0.038	0	0.038	0.004	0.007	0.024	0.063	0.01
T11	0.01	0.011	0.011	0.01	0.01	0.061	0.024	0.007	0.004	0.038	0	0.038	0.004	0.007	0.024	0.061
T12	0.063	0.01	0.011	0.011	0.01	0.01	0.063	0.024	0.007	0.004	0.038	0	0.038	0.004	0.007	0.024
T13	0.024	0.061	0.01	0.011	0.011	0.01	0.01	0.061	0.024	0.007	0.004	0.038	0	0.038	0.004	0.007
T14	0.007	0.024	0.061	0.01	0.01	0.011	0.01	0.01	0.061	0.024	0.007	0.004	0.038	0	0.038	0.004
T15	0.004	0.007	0.024	0.061	0.01	0.01	0.011	0.01	0.01	0.063	0.024	0.007	0.004	0.038	0	0.038
T16	0.038	0.004	0.007	0.024	0.061	0.01	0.01	0.011	0.01	0.01	0.063	0.024	0.007	0.004	0.038	0

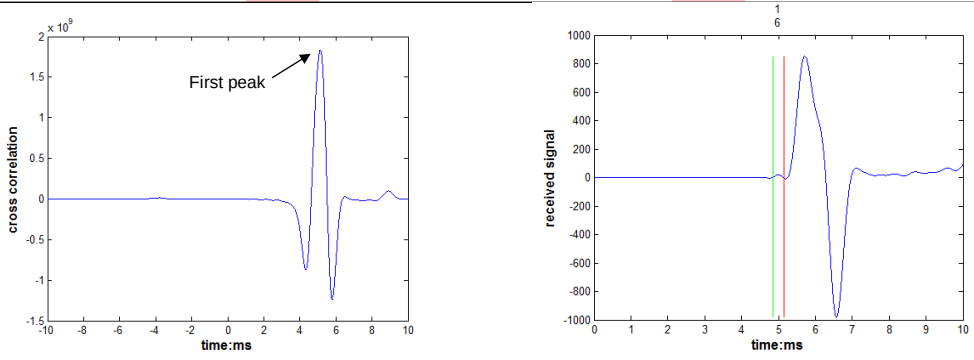

(a) (b)

Figure 4. Cross-correlation (a) and received signal (b) between transmitter No.1 and receiver No.6

One way to solve this problem is to choose a narrower pulse as the excitation signal. It is proved that the width of cross-correlation envelops equals to twice reciprocal bandwidth. Therefore, the width of the excitation signal main lobe should be smaller than the minimum difference between direct wave and reflection of delay time $\Delta\tau$.

A coarse estimation of $\Delta\tau$ is based on the highest sound speed, $c = 1200\ \mathrm{m/s}$ when temperature is 4000K. The minimum ray length difference between direct propagation and reflection is 9.4mm, so that $\Delta\tau = 7.8 * 10^{-6}\ s$ and the corresponding bandwidth for the excitation signal is $B = \frac{2}{\Delta\tau} = 257\ KHz$, which is too strict and not practicable. In fact, we can only focus on reducing estimation error larger than 5%, as is shown in Table 1, where $\Delta\tau = 0.93 * 10^{-4}\ s$ and corresponding bandwidth are $B = \frac{2}{\Delta\tau} = 5.38\ KHz$. However with a narrow bandwidth of 5.38 kHz there will be severe distortion in received signal, as is shown below in Figure 5(b), that it is difficult to find the TOF point on the cross-correlation series Figure 5(a). Basically from simulation it is found that B= 1 kHz is the widest bandwidth, distortion can be avoided and comparatively good resolution is obtained in time domain.

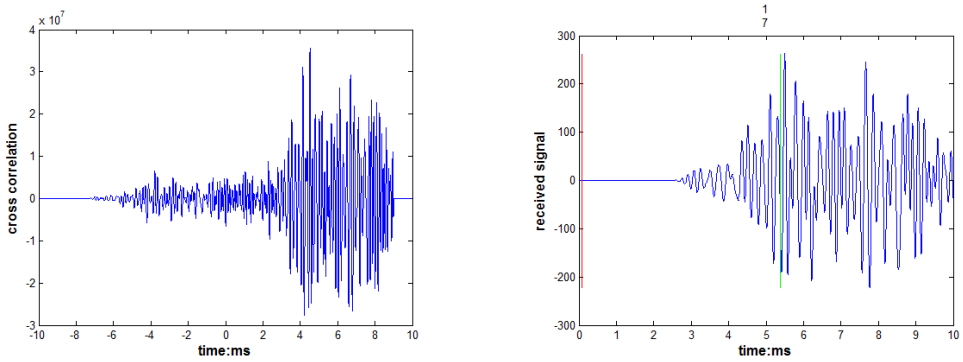

(a) (b)

Figure 5. Bandwidth B $= 5.38KHz$, cross-correlation (a) and received signal (b)

4 RECONSTRUCTION

Temperature field reconstruction can be considered as solving an inverse problem, which is to derive the slowness of sound speed s from TOF measurements. AT does not have many TOF data due to the limited measurements. Here 16 sensors are placed around the region of interest and give only 120 independent ray paths of wave propagation, which means 120 TOF measurements per image. If the whole sensing area is divided into 40*40 grids, 1600 unknown parameters must be estimated from these limited TOF data. That is why a modelling step is critical to use fewer parameters to approximate the original field.

A weighted sum of radial basis functions (RBF) is adopted to model the slowness of sound wave propagation (Wiens 2009). Suppose there are K number of RBFs, and all of these basis contributes to the slowness at each grid, which is shown as:

$$s(\boldsymbol{x_i}) = \sum_1^K w_{i,k} e^{-\beta \|\boldsymbol{x}_i - X_{b,k}\|} \tag{9}$$

where x_i is the center of i-th grid, β is a scaling factor and $w_{i,k}$ is the weights for k-th basis function on i-th grid. In this simulation as no further prior knowledge is given, all the basis center $X_{b,k}$ is uniformly distributed inside the area. Then this modelling process is rewritten in a matrix form as:

$$s = Bw \tag{10}$$

The inverse problem described in Equation (6) $g = As$ becomes

$$g = ABw = \Phi w \tag{11}$$

Then we apply Tikhonov regularization is applied to minimise the following function

$$\|g - \Phi w\|^2 + \eta \|w\|^2 \tag{12}$$

In order to extract unknown w from TOF measurement data g, Truncated Singular Value Decomposition (TSVD) is used. First the system mapping matrix Φ is decomposed as:

$$\Phi = U \Sigma V' \tag{13}$$

Afterwards weight the small singular value in Σ, which is a smooth regularization and keeps the m largest elements $\lambda_1, \lambda_2, \lambda_3 \ldots . \lambda_m$ left for reconstruction. At last, the regularization factor η is applied to weight all the elements λ_i, and $\hat{w}$, an estimated solution to (12) is:

$$\hat{w} = \sum_1^m \frac{{\lambda_i}^2}{{\lambda_i}^2 + \eta} * \left(g^{'} * u_i * v_i\right) \tag{14}$$

The modified TSVD method filters the high-frequency components using η to weight all the elements λ_i, which gives a similar solution to the Tikhonov regularization methods.

5 SIMULATION RESULTS AND DISCUSSION

The simulation includes two steps: the forward problem and the inverse problem. As described in Section 2, COMSOL Multiphysics generates temperature field and simulates the time-dependent pressure acoustic field. The TOF picker based on cross-correlation detection extracts the TOF measurements from the received pressure acoustic signals. Then using RBF modelling and TSVD methods to reconstruct the temperature field.

Recall that simplified linear equation $g = ABw$, as *A* is the system matrix which element is the segment length for each ray path in every grid. *B* is the modelling matrix defining a linear transform to use much fewer parameters to represent the temperature field, here we use the RBF network. And *g* is TOF data measurements and s is the vectorised slowness field. The total reconstruction error can be considered as:

$$e = \|s - \hat{s}\|^2 = \|s - B\widehat{w}\|^2 \tag{15}$$

where $\widehat{w} = min_{\hat{r}}\|(g+n) - AB\widehat{w}\| = V_\Phi {\Sigma_\Phi}^{-1} {U_\Phi}'(g+n)$ and $A = \Phi = U_\Phi \Sigma_\Phi {V_\Phi}^{'}$; $\hat{s}$ is the reconstructed slowness distribution, $\hat{s} = B\widehat{w}$; n is the noise term in the TOF measurement.

If the TOF error n is ignored here, thus only error caused by reconstruction algorithm is considered here, the total reconstruction error e is split into two parts: approximation error e_m and calculation error e_c. The approximation error is defined as $e_m = \|s - Bw^*\|$, where $w^* = min_{r^*}\|s - Bw^*\| = V_B {\Sigma_B}^{-1} {U_B}'s$. This is the process to find w^* and s^* that best fit the temperature field given linear mapping matrix *B*. The calculation error is defined as $e_c = \|s^* - B\widehat{w}\|$, where $\widehat{w} = min_{\widehat{w}}\|g - AB\widehat{w}\|$is extracted from the measurements. Three errors are rewritten as:

$$e = \|s - B\widehat{w}\| = \|s - Bw^* + Bw^* - B\widehat{w}\| \le e_m + e_c \tag{16}$$

$$e_m = \|s - Bw^*\| = \left\|s - BV_B {\Sigma_B}^{-1} {U_B}^{'} s\right\| \tag{17}$$

$$e_c = \|s^* - B\widehat{w}\| = \left\|BV_B {\Sigma_B}^{-1} {U_B}'s - BV_\Phi {\Sigma_\Phi}^{-1} {U_\Phi}'g\right\| \tag{18}$$

To validate the overall performance of AT, three cases representing different temperature field of the furnace are studied below. **Case 1**: a temperature field with a large temperature fluctuation range from 293.15 K to 2600 K, with a comparatively sharp peak close to the furnace boundary. **Case 2**: a temperature field with a smaller temperature fluctuation range from 293.15 K to 1000 K, without any obvious peak in the sensing area. **Case 3**: a flat temperature field without any fluctuation, all the pixels has the same temperature of 293.15 K, as for the situation when furnace is not working.

The total reconstruction error includes the measurement error from TOF picker, the approximation error of RBF modelling of the temperature field and the calculation error using TSVD to solve the inverse problem. The reconstruction errors of three cases are listed in Table 2.

Table 2. Relative reconstruction error of three cases

	Slowness approximation error	Slowness calculation error	Slowness reconstruction error	temperature reconstruction error
Case 1	0.0681	0.0857	0.0956	0.191
Case 2	0.0353	0.0403	0.0476	0.0953
Case 3	3.4180e-06	0.0106	0.0104	0.0210

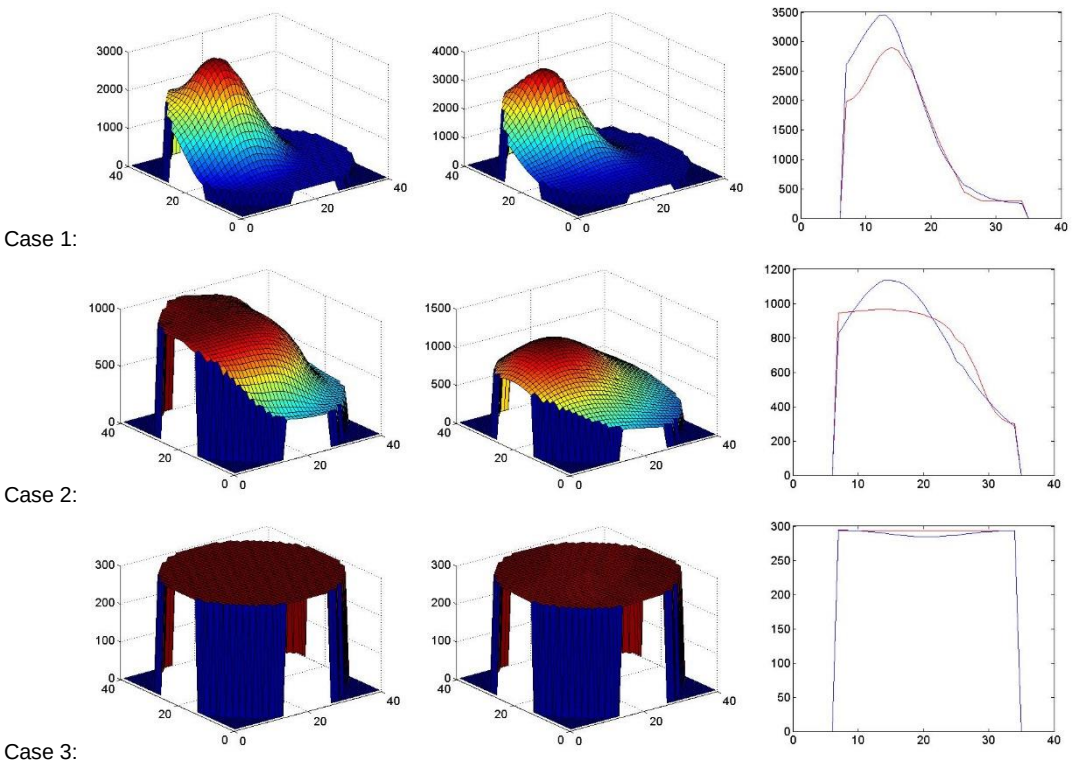

Figure 7. Original temperature field (left), reconstruction results (right) and comparison along diagonal (red indicate original temperature and blue is the reconstruction results)

The results show the reconstruction error is highly dependent on the temperature field fluctuation. For the room temperature field (case 1) and the flat one (case 2), results both show good reconstruction quality. However for temperature field with sharp peaks (case 3), the reconstruction error rate is 19.1%.

6 CONCLUSION

In this paper, the simulation work of acoustic tomography system for monitoring temperature field is studied. The forward problem is solved by COMSOL Multiphysics and cross-correlation TOF picker is used to estimate Time-of-Flight (TOF) measurements between received and received acoustic signal. Reconstruction algorithm using Radial Basis Functions (RBF) represents and Truncated Singular Value Decomposition (TSVD) methods are also introduced to recover the temperature field of three different simulation cases. The reconstruction error is analysed and it can be concluded that the proposed algorithm can provide a quantitative estimation with a relative error of 9% on a smooth temperature field, where the variation of temperature is from 293.15 K to 1000 K. Whereas, when the fluctuation is comparatively large, varies from 293.15K to 3500 K, the reconstruction error is increased to 19%. To further improve the performance of temperature field reconstruction, the bent ray model can be used instead of the straight ray model, namely, taking the refraction effect into account. Besides, the time-dependence property of temperature field can be utilised by applying a spatiotemporal sampling to the temperature field, this will help to solve the limited-data problem of acoustic tomography and improve the reconstruction quality. In addition, statistical-based algorithms will be used to solve the tomography inverse problem, as it shows superiority in undetermined problems over algebraic-based algorithms used in this paper.

7 REFERENCES

CHUNCHOZOV, I. P., OTREZOV, A. I., PETENKO, I. V., TOVCHIGRECHKO, V. N., SVERTILOV, A. I., FOGEL', A. L., AND FRIDMAN, V. E. (1997). Travel-time and duration fluctuations of acoustic

pulses in the atmospheric boundary layer. Izvestiya Atmospheric and Oceanic Physics, 33(3), 293-307.

JOVANOVIC.I, L.SBAIZ, AND MARTIN VETTERLI, (2006), "Acoustic tomography method for measuring temperature and wind velocity." Acoustics, Speech and Signal Processing, 2006. ICASSP 2006 Proceedings. 2006 IEEE International Conference on. Vol. 4. IEEE.

LIU, Y., LIU, S., LEI, J., LIU, J., SCHLABERG, H. I., AND YAN, Y. (2015). A method for simultaneous reconstruction of temperature and concentration distribution in gas mixtures based on acoustic tomography. Acoustical Physics, 61(5), 597-605.

LI, C., HUANG, L., DURIC, N., ZHANG, H., AND ROEW, C. (2009). An improved automatic time-of-flight picker for medical ultrasound tomography. Ultrasonics, 49(1), 61-72.

MUNK, WALTER, AND CARL WUNSCH, (1982), "Observing the ocean in the 1990s."Philosophical Transactions of the Royal Society of London A: Mathematical, Physical and Engineering Sciences 307.1499: 439-464.

RJENSTRA, SJOERD W., AND AVRAHAM, (2003), "An introduction to acoustics." Eindhoven University of Technology 18: 19.

ROGERS, K., AND FINN, A. (2013). Three-dimensional UAV-based atmospheric tomography. Journal of Atmospheric and Oceanic Technology, 30(2), 336-344.

SPIESBERGER, JHON L., AND KURT M. FRISTRUP, (1990). "Passive localization of calling animals and sensing of their acoustic environment using acoustic tomography." American Naturalist: 107-153.

WIENS, TRAVIS AND Paul.T, (2009), "Turbulent flow sensing using acoustic tomography." Proceedings of Innovations in practical Noise Control 2009.
WILSON, K. AND THOMSON, D. W., (1994), "Acoustic tomographic monitoring of the atmospheric surface layer." Journal of Atmospheric and Oceanic Technology 11.3: 751-769.

ZIEMANN, A., K. ARNOLD, AND A. RAABE, (1999), "Acoustic Travel Time Tomography–A Method for Remote Sensingof the Atmospheric Surface Layer."Meteorology and Atmospheric Physics 71.1-2: 43-51.